Space Object Characterization with 16-Visible-Band Measurements at Magdalena Ridge Observatory

Abstract

Data was collected at the Magdalena Ridge Observatory (MRO) with the Multi Lens Array (MLA) camera coupled to the MRO 2.4 m telescope. MRO is located at 33.985°N, 252.811°E at an altitude of 3193 m, approximately 30 miles West of Socorro, NM. The MRO facilities are intended for both astronomical research and Resident Space Object (RSO) characterization. The purpose of the measurement campaign was to collect both resolved images and unresolved signatures of RSOs in 16 spectral bands, ranging from 414 nm to 845 nm. During the campaign, observations were made over five sessions for the period 21-27 September 2007. During that time we succeeded in observing and collecting data for 18 different calibration stars and 40 different RSOs, mostly those in Low Earth Orbit (LEO). A major objective of the measurement campaign is to collect RSO data that can be used to select spectral bands optimized for estimating surface material composition. The analysis results help determine the nominal spectral differences for typical RSO materials. The paper will discuss the potential of using a multiband camera for RSO identification and characterization.

Phan D. Dao[*], Patrick J. McNicholl, James H. Brown, Justin E. Cowley, Mike J. Kendra and Peter N. Crabtree, *Air Force Research Laboratory, Space Vehicles Directorate*
Anthony V. Dentamaro, *Boston College*
Eileen V. Ryan, William Ryan, *Magdalena Ridge Observatory*

Classification: Unclassified
Category: Non-resolved Object Characterization.

1. Introduction and background

The Air Force Research Laboratory Space Vehicles Directorate (AFRL/RV) and its Space Object Surveillance Technologies (SOST) Program have a mission to develop sensing methods and analytical approaches that will exquisitely characterize Resident Space Objects (RSOs) for space-to-space observations. The measurements and analyses presented in this paper demonstrate techniques to classify materials in resolved images and identify objects with unresolved light curves, both with the use of two spectral bands in the visible.

The Space Surveillance Network has the critical mission of maintaining the catalog of space objects. In addition to the metric data used for constructing orbital information, photometric and radiometric data is also used for Space Object Identification (SOI). For many years, photometric data consisted of broadband light curves where most of the information is carried in their temporal variations. Lambert [1] used LWIR spectral signatures to investigate specifically the solar panels. It has been suggested by Payne [2], through modeling and simulation, that broadband color indices could be used for identification. Systematic selection of filter bands for SOI and Space Situational Awareness (SSA) has been studied first and reported by the Air Force Maui Optical and Supercomputing (AMOS) site research group [3]. In these studies, the authors used spectrally resolved light curves collected on satellites to develop a technique to identify them based on the combination of magnitude, colors and solar phase angle. A spectrograph provided the spectrally resolved signature. The selection of filters was however based on the maximum difference of medians of in-band intensities. In-band intensities were constructed from the resolved spectrum. Their idea was to select the two wavelengths for which the spans of the median intensities –among the classes of observed satellites- show local maxima, hence identifying a pair of bands that will maximize the differences in the intensities from different satellites. While the SOI-In-Living-Color (SILC) technique was shown to successfully classify satellites, especially those used in the study, the use of median span as an indicator of pair-wise class distinguishability cannot be rigorously justified. There are many differences between that procedure and ours, but the most important one is the method of rigorously selecting the bands. We apply the concepts of statistical distance of the Mahalanobis [4] and Bhattacharyya [5] functions to the classification of material and satellites. The Mahalanobis distance is used to determine the likelihood that an observed flux corresponds to a class of material when an *a posteriori* probability distribution exists. We also apply these tools to the problem of satellite

Report Documentation Page

1. REPORT DATE **SEP 2008**	2. REPORT TYPE	3. DATES COVERED **00-00-2008 to 00-00-2008**

4. TITLE AND SUBTITLE	5a. CONTRACT NUMBER
Space Object Characterization with 16-Visible-Band Measurements at Magdalena Ridge Observatory	5b. GRANT NUMBER
	5c. PROGRAM ELEMENT NUMBER
6. AUTHOR(S)	5d. PROJECT NUMBER
	5e. TASK NUMBER
	5f. WORK UNIT NUMBER

7. PERFORMING ORGANIZATION NAME(S) AND ADDRESS(ES) **Air Force Research Laboratory,Space Vehicles Directorate,3550 Aberdeen Ave SE,Kirtland AFB,NM,87117**	8. PERFORMING ORGANIZATION REPORT NUMBER

9. SPONSORING/MONITORING AGENCY NAME(S) AND ADDRESS(ES)	10. SPONSOR/MONITOR'S ACRONYM(S)
	11. SPONSOR/MONITOR'S REPORT NUMBER(S)

12. DISTRIBUTION/AVAILABILITY STATEMENT
Approved for public release; distribution unlimited

13. SUPPLEMENTARY NOTES
2008 Advanced Maui Optical and Space Surveillance Technologies Conference, 16-19 Sep, Maui, HI.

14. ABSTRACT
Data was collected at the Magdalena Ridge Observatory (MRO) with the Multi Lens Array (MLA) camera coupled to the MRO 2.4 m telescope. MRO is located at 33.985oN, 252.811oE at an altitude of 3193 m, approximately 30 miles West of Socorro, NM. The MRO facilities are intended for both astronomical research and Resident Space Object (RSO) characterization. The purpose of the measurement campaign was to collect both resolved images and unresolved signatures of RSOs in 16 spectral bands, ranging from 414 nm to 845 nm. During the campaign, observations were made over five sessions for the period 21-27 September 2007. During that time we succeeded in observing and collecting data for 18 different calibration stars and 40 different RSOs, mostly those in Low Earth Orbit (LEO). A major objective of the measurement campaign is to collect RSO data that can be used to select spectral bands optimized for estimating surface material composition. The analysis results help determine the nominal spectral differences for typical RSO materials. The paper will discuss the potential of using a multiband camera for RSO identification and characterization.

15. SUBJECT TERMS

16. SECURITY CLASSIFICATION OF:			17. LIMITATION OF ABSTRACT	18. NUMBER OF PAGES	19a. NAME OF RESPONSIBLE PERSON
a. REPORT **unclassified**	b. ABSTRACT **unclassified**	c. THIS PAGE **unclassified**	**Same as Report (SAR)**	**10**	

identification. Some of the data taken at Magdalena Ridge Observatory (MRO) is from large space objects for which the images are resolved. With this data, we attempt to classify material based on spectral difference and intensity. The Bhattacharyya distance is used to measure the distinguishability between two statistical classes. That distance is to be maximized by the choice of observational variables, quantities derived from in-band intensities and from other observational parameters. For each class of satellites, observational or simulated data can be obtained to form the *a posteriori* data (*a priori,* in the case of simulated data) that specifies the classes. As with the SILC work, we propose to use multiband signatures. The 16-band visible sensor, as mounted on the MRO telescope provided data used to validate our concept and to conduct the band selection. The bands completely cover the operational range of a typical CCD sensor. The average pair-wise Bhattacharyya distance, calculated for each pair of bands, is used to select the bands. The highest average pair-wise distance warrants the best chance to distinguish the classes. The Mahalanobis distance is used to determine whether a set of in-band intensities belongs to a particular class.

2. Magdalena Ridge Observatory telescope

The MRO's fast-tracking 2.4-meter telescope (see Figure 1) is a new high-technology facility located at 10,612 feet atop the Magdalena Mountains in Central New Mexico [33° 59' 6.0" N, 107° 11' 21.0" W], and is part of the New Mexico Institute for Mining and Technology - a small research and engineering university. The MRO 2.4-meter is one of the largest telescopes in the world that has as its primary mission the physical characterization of small bodies (both natural and artificial) in the Solar System. The 2.4-meter's control system is designed to provide convenient and accurate non-sidereal tracking, and the telescope is capable of rapid movement (slew rates are up to 15 ^{o}/sec) making it an ideal instrument for studying fast moving RSOs. The 2.4-meter telescope can accommodate a wide variety of instrument systems, and supports the fabrication, integration, and operation of new instrumentation as well as the development of new and innovative observational techniques.

Figure 1. Magdalena Ridge Observatory 2.4 m tracking telescope.

The telescope is a modified Ritchey-Chrétien design, with an overall focal ratio of f/8.9 and an unvignetted Field-of-View (FOV) of 15 arc-minutes. The intrinsic resolution of the optical system is defined by a full-width half-maximum (FWHM) of 0.2 arc-seconds for a point source. There are two Nasmyth ports (which can support larger and heavier instrumentation) and four bent Cassegrain ports, one of which permanently hosts a Shack-Hartmann wavefront sensor to facilitate automatic collimation and focusing. Therefore, the facility can simultaneously mount up to 5 instruments at any given time. Median good seeing at the site is 0.7 arc-seconds, and the faintness limit of the telescope for visual wavelengths is about 25th magnitude. For the observations using the Multi Lens Array (MLA) camera, the Low Earth Orbit (LEO) objects were initially located by pointing the telescope along a track calculated from recent two-line elements (TLE). The precision of these elements was usually sufficient to detect the object in a 12-inch Acquisition Telescope (AT) mounted on the main telescope, which has a FOV of about 0.5 degrees.

3. 16-band visible lenslet array sensor

The sensor--designed and built by Solid State Scientific Corporation (SSSC) --employs a proprietary optic with an array of 16 filter-optic combinations. The reimaging optics share the available input aperture and the images produced by them share a single interline transfer CCD to produce 16 spectrally filtered and temporally synchronous sub-images (Figure 2). In principle, such a device is capable of achieving the same duty cycle as conventional full aperture filter-switching cameras. It trades off the potential advantages of the larger etendue of a full aperture spectrally filtered imaging implementation (e.g., resolution and/or field-of-view) in order to achieve synchronous spectral imaging of objects with high frequency light curves. Technical details of the sensor are SSSC proprietary information.

In order to employ the existing prototype of this technology--which was intended for standalone operation-- coupling optics were designed and built by SSSC to re-image the focal plane of the MRO 2.4 m telescope. Because

the coupling optics focus the input aperture of the telescope onto that of the MLA camera, the telescope's central obscuration partially vignettes the central four sub-images.

4. Target selection and campaign (Jim, Mike, Justin and MRO)

A collaboration between the AFRL SOST program, the Magdalena Ridge Observatory (MRO), and SSSC was formed to acquire multiband temporal light curves of observable RSOs for the purpose of characterizing RSOs from their resolved and unresolved signatures. A unique 16-band visible spectral imager from SSSC was coupled with the MRO 2.4 m telescope to observe Low-Earth Orbiting (LEO) RSOs. The unique combination of telescope and sensor design allowed for tracking dim unresolved LEO objects. Together with spectral information, the temporal data offered an opportunity for exquisite characterization, including motion, materials, and spatial/temporal changes.

The experiment schedule extended over 8 days, spanning September $20^{th} - 27^{th}$, during which time approximately 104 data collects were obtained. These collects included star calibrations, dark current, and other calibration measurements. Approximately 67 of the 104 data collects were obtained for hard target bodies. Some of these were not analyzed due to clouds or other anomalies in the measurements.

Figure 2. Example Image Array: Data from ISS (25544) transit covered from MRO on 09/27/2007.

The experiment provided for simultaneously gathering the band images at temporal frame rates from 2 to 200 Hz. The 16 visible colors and light curve signatures provide a means for characterizing size, shape, motion, and composition of unresolved RSO images. The SSSC sensor was developed under a SBIR contract to the Army's Armament Research, Development and Engineering Center. It is small, lightweight and has a 9° FOV. Figure 2 above shows a single image frame of the ISS for the 16 simultaneous co-registered band images for a point in time. Unlike the resolved image above, however, the experiment was aimed at gathering unresolved point source imagery.

MRO was responsible for telescope operations and recording precision satellite positions with precise timing. AFRL and MRO provided radiometrically accurate spectra for the calibration stars. SSSC was responsible for operation of the sensor including data acquisition, data storage, and data reduction. Analyses concentrated on identifying and characterizing the observed satellites from the temporal signatures of their unresolved optical signals. The 16 visible bands provided spectral information that allowed material property unfolding and, therefore, unique features important to characterization. Apart from the telescope, SSSC provided most of the supporting equipment needed for the experiment, including a lens coupler, IPX-VGA210 camera, 640 x 480 KAI-0340 detector (on the IPX-VGA210 camera), two 300 GB USB 2.0 external hard drives, eighteen 320 GB USB 2.0 external hard drives, and the 16-band MLA optics. Table 1 lists the filter specifications.

Band#	λ_c	FWHM	Band#	λ_c	FWHM	Band#	λ_c	FWHM	Band#	λ_c	FWHM
1	430.5	33	5	542.5	41	9	623.5	41	13	746.5	41
2	449.0	36	6	550.0	38	10	630.0	38	14	763.5	41
3	477.0	36	7	589.0	40	11	656.0	38	15	797.0	34
4	500.0	36	8	615.0	42	12	729.5	37	16	826.5	37

Table 1. Specifications of optical filters

An amateur observer site (http://www.heavens-above.com) was used to obtain satellite visibility predictions for the MRO measurements. Predictions of magnitude 8 and brighter LEO objects from the Heavens-Above site were used in determining which objects to measure. TLEs were obtained for the most observable objects, generally rocket bodies. Typically there were 10-20 objects passing over the MRO site during each dawn/dusk condition spanning a period of 2-3 hours that were selected for observation.

For star and unresolved images, the digital values of the pixels are integrated over a 2x2 or 3x3 pixels area. Because of atmospheric effects, the registration of the pixels shows time variation but the spatial jittering is typically less than one pixel. For this particular study, only relative calibration is required, and it was achieved by calculating the multiplication factors that force the in-band intensities to agree with published calibration curves using the following stars: SAO31899, HR7596, HR337 (3350K), HR8634 (8000-10000K), and HR1457 (Aldebaran:4100K). It is assumed that changing atmospheric absorption does not affect the relative calibration since there is no pronounced atmospheric absorption in this window. The calibration factors are shown in Figure 3. The error bars in four of the 16 bands are much higher than typical values because the corresponding sub-apertures are partially blocked by the secondary mirror, and the throughputs are therefore quite low.
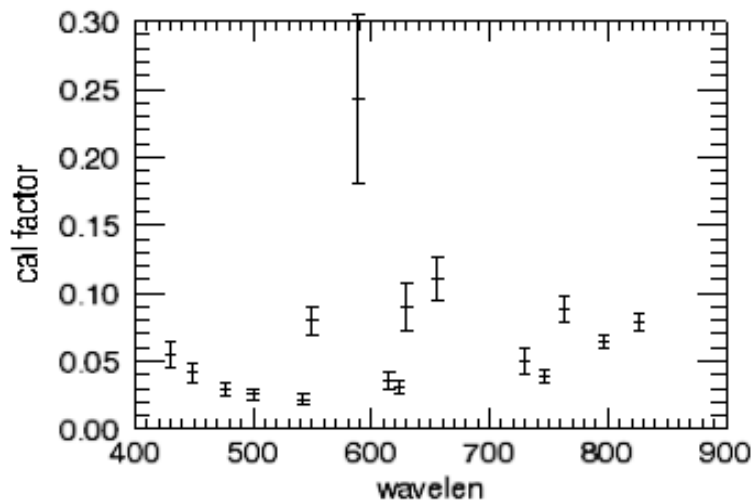

Figure 3. Relative calibration factors.

Figure 4 shows an example of the light curve at the 477 nm band and the spectral difference between that and the red band at 746 nm. The light curves were collected for Helios-1B (Sat No. 25977) on 25 Sept 2007 starting at 11:07:46 UT, and in the plots, band B is centered at 477 nm and band R centered at 746 nm. The normalized spectral difference, (B-R)/(B+R), is in the bottom panel.

5.   Results and discussions: material identification and confirmation

The goal of this research effort is to develop a technique for identifying materials based on observations at multiple bands and *a priori* spectral reflectance information. For that to happen, it should be shown first that different materials generally show different spectral reflectance profiles, and that the difference can be specified by a small number of bands. In this demonstration, a few distinct (material) points on the ISS body are chosen for analysis, and we show that the body points yield distinguishable characteristics.
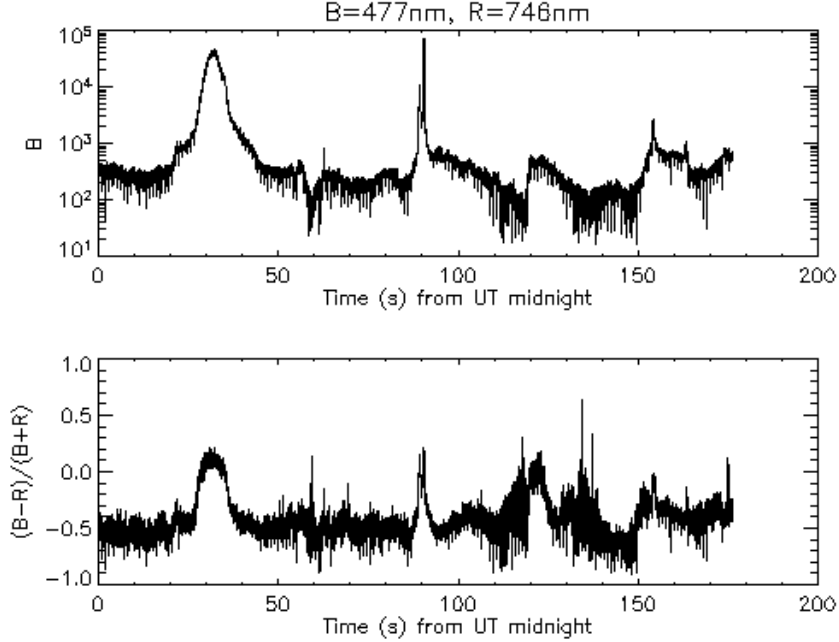
Figure 4. Helios-1B light curve (top) and normalized spectral difference curve (bottom).

The ability to distinguish materials derives from the ability to associate the measurement with membership to a particular class. Data points are represented by coordinates in a multidimensional space, hence referred to as the feature space. Which in-band signals or derived quantities are to be used as coordinates is the subject of later discussions. In the feature space, the ability to identify a material or space object depends on the anticipation that data points belonging to the same class of material or class of satellite are grouped together and hopefully separated from the loci of other classes. Material identification can be achieved with resolved images and object identification with non-resolved light curves. The grouping of class points may not have a strictly Gaussian distribution, but in this study we assume that the distributions are compact enough to use a formalism developed for Gaussian distributions. In the feature space, the Bhattacharyya statistical distance (B distance) is used to determine the distinguishability of two classes. This function is commonly used in image analysis and terrestrial remote sensing [6]. The B distance is defined as follows:

$$B = \frac{1}{8}(\mu - \mu')^T \left(\frac{\Sigma + \Sigma'}{2}\right)^{-1}(\mu - \mu') + \frac{1}{2} \cdot \ln\left(\frac{|\Sigma + \Sigma'|}{2 \cdot \sqrt{|\Sigma| \cdot |\Sigma'|}}\right) \tag{1}$$

where μ is the mean vector of the first class, and μ' is that of the second class. In other words, μ is the center of mass of the class. Σ and Σ' are the corresponding covariance matrices of the measurement vectors **X** and defined as follows:

$$\Sigma_{i,j} = E\left[\left(\overrightarrow{X_i} - \mu_i\right) \cdot \left(\overrightarrow{X_j} - \mu_j\right)^T\right] \tag{2}$$

In Equation 2, **X** is a vector of variables and it has as many components as the number of coordinates used to represent a measurement on the feature space. If each measurement can be represented by two variables, e.g. derived from two in-band intensity levels, **X** has two components: X and Y. Each variable can assume as many values as the number of measurements. In Equation 2, the indices i and j can take the values 1 or 2. The covariance matrix Σ is of size 2x2. The expectation value E is computed using all the values assumed by variables X and Y. The first term in the expression of Bhattacharyya distance is analogous to the squared average of the Mahalanobis distance, and the second term reflects the difference in covariance matrices for the two classes. The following characteristics of the B distance are crucial to our technique. First, it is scale invariant, so we are free to choose the variables. Second, it

allows the class distributions to be non-spherical, for instance ellipsoidal, if required. In other words, the probability that a measurement point belongs to a class depends not only on the distance from the center of mass, but also on the relative direction. The B distance is a good representation of the statistical separation between two classes. It will be used as a metric of how distinguishable one class is relative to another. It will also be used to select the optical bands for maximum class separation.

A multiband intensity signal can be represented as a vector of variables. A two-band measurement can be represented as a point whose coordinates are the intensities or linear combinations of intensities at their respective bands. Figure 5 shows the location of three points on the ISS body for which we make measurements. In Figure 6, we plot the position of a measurement using the coordinates X and Y. In Figure 7, we plot the histogram of the observation points. The two-dimensional histogram is similar to the (number) density distribution. In this plot, for each observation, the coordinates X and Y are defined as follows:

$$X = B + R \tag{3}$$

$$Y = (B\text{-}R)/(B\text{+}R) \tag{4}$$

In the expressions for X and Y, B is the range-corrected intensity measured in the band of shorter wavelengths and R the range-corrected intensity measured at longer wavelengths. When the orbit is known, the solar phase angle, Z, can be calculated and used as the third variable. We claim that X and Y can be used to identify surface material on the ISS body, and that the addition of Z improves the identification. To validate this claim, we select three points on the ISS and record the intensities in all 16 bands for the entire pass. The frame rate used in this session is 80 Hz. Since over the course of the track, the look angle changes substantially, the point selected on the images may not be exactly the same point on the ISS body. The intent is to analyze the light curves of what appears to be at the same place on the body or, at least, having the same surface material. It is possible that the probed point has moved from one side of the cylindrical body to the other during the pass. The (X,Y) data points are for those that correspond to the ISS body points shown in Figure 5. There were 11951 video frames recorded during the pass that started 12:38:52 UT and ended 12:41:12 UT. Of those frames, 732 frames are eliminated due to poor SNR. Therefore each body point will be shown as 11219 different points on the plot.

In Figure 6, the measurement points are shown in the 2-D space for 3 pairs of center wavelengths. In the leftmost panel, 477 and 746 nm, the points seem to group themselves in three clouds with some overlap between clouds #2 (green) and #3 (red). Cloud #1 (black) is clearly separated from the other two. In the middle panel, 500 and 729 nm, cloud #3 is seen broken up into two clumps, and there is some overlap between clouds #2 (green) and #3 (red). In the rightmost panel, 449 nm and 763 nm, there is again some overlap between clouds #2 (green) and #3 (red). In addition, there is noticeably less separation between clouds #1 and #2 as compared to the leftmost panel. The B distances, computed for each pair of classes (body points), are shown on the plot and also in Table 2. It should be noted that the table only includes the pairs of bands that give highest separation of classes. The 477/746 nm pair has, by a small margin, the highest average B distance. In Figure 7, the number density of measurement points in the feature space is shown for the 477/746 nm band pair.

Though we did not proceed to identify materials using the described technique, the result shows that different locations on the ISS yield spectral information that can be mapped to points which are distinguishable in the feature space. To actually implement this technique, multiband data from measurements or simulation would be used to define the classes in the feature space. Each measurement will be mapped to the feature space, and with the assumption of normal Gaussian distribution, the probability that measurement **X** belongs to class i can be calculated as follows:

$$p(i \mid X) = \frac{p(i)}{p(X)(2\pi)^{n/2} |\Sigma_i|^{1/2}} e^{\left[-\frac{1}{2}(X - \mu_i)^T \Sigma_i^{-1} (X - \mu_i) \right]} \tag{5}$$
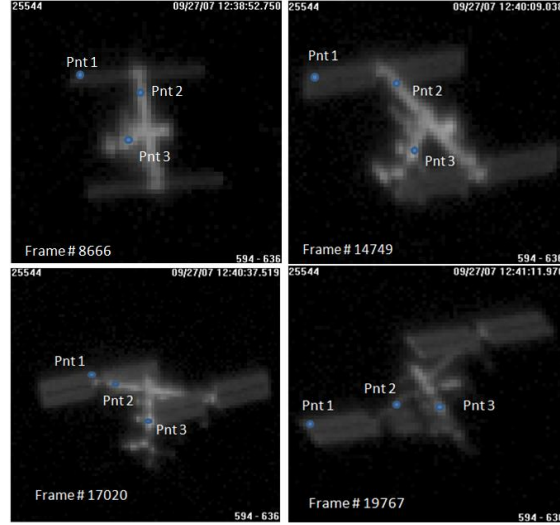
Figure 5. Points on ISS body where in-band intensities are analyzed.

Table 2 lists the B distances between classes for the most promising pairs of bands: 477/746, 500/729 and 449/763. For each pair of bands, the measurement at a body point at a given time yields a triplet of values: B, R and solar phase angle. Each measurement is mapped into a point in the 2D or 3D feature space. In this space, a body point is represented by a distribution of points, (X,Y) or (X,Y,Z). Fortunately, there are bands that can be chosen such that the measurements are transformed into conglomerates (or clouds) of points in the feature space. In those cases, the measurements in one pass generate a cloud for each body point. There are three clouds in the feature space (Figure 8) for three body points. In Table 2, P1-P2 is the distance between cloud #1 and cloud #2, and so on. Clouds which are separated by a large B distance are distinguishable. With an independent measurement, one can associate it with a particular class.

Dimension	Center 1 (nm)	Center 2 (nm)	P1-P2	P2-P3	P1-P3	Avg. B distance
2	477	746	2.827	0.851	3.343	2.341
2	500	729	2.558	0.837	3.397	2.264
2	449	763	1.976	0.775	3.072	1.941
3	477	746	3.385	1.265	4.149	2.933
3	500	729	3.226	1.277	3.940	2.814
3	449	763	2.619	1.179	3.676	2.491

Table 2. Bhattacharrya separation between classes.

It is noted that the B distance between P2 and P3 is only 0.85 for the 2D clouds, while the addition of solar phase angle improves the distance to 1.26. This improvement is confirmed in Figure 8 where the three clouds are shown in the 3D feature space. The projection of the clouds onto the XY plane, similar to the scatter plot shown Figure 7, is also shown. In comparing the projection with the 3D images of the three clouds, it is noted that cloud #2 and #3 are more separable with the addition of the third dimension which is based on the object's solar phase angle.

In general, the representation of the measurements in the 2D and 3D feature space, as described in this paper, makes it possible to determine quantitatively the distinguishability of the various body points. In future works, we will attempt to identify material in RSO resolved images using the same formulation of statistical distance.

6. Results and discussions: satellite identification

The uniqueness of the sensor is its ability to record images at fast frame rates and without time multiplexing for all band measurements. As seen in Figure 4, RSO light curves can present a challenge to a multiband sensor that relies on filter wheels when dealing with glints. We claim that the spectral content of glints contains valuable

information about the surface of reflection. Glints are generally more intense and we speculate that their spectral signature uniquely identify the RSO. Figure 9 shows the simulation in the 2D feature space (top) and the measurements of Helios-1B (Sat No. 25977) on 25 Sept 2007. It is encouraging to observe a band of points with high intensities and spectral difference which is slightly positive. These points of high intensities are presumably glints which would asymptotically approach a fixed Y value. The Y value is representative of the material of the reflective surface. In this case, Teflon was used in the simulated Helios and we confirmed that the glint in the simulation is caused by a cylinder made of Teflon. However, it is quite clear that there are two more bands of glints with negative asymptotes which were not observed in the data. Future investigations will focus on the discrepancies.
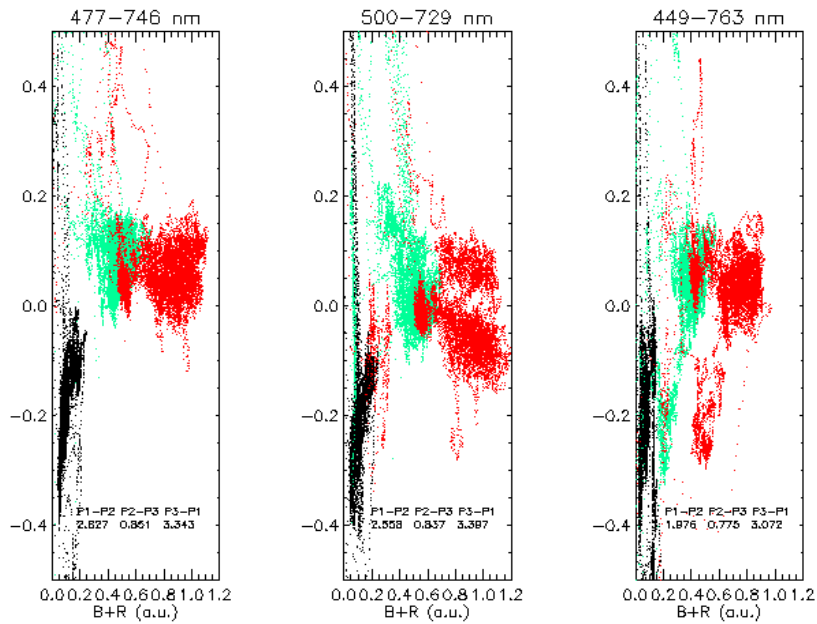
7. Acknowledgements

Figure 6. Scatter plots of measurement points when X and Y are defined as in Equations 3 and 4. Listed are the center wavelengths of the B and the R bands. The point distributions are color-coded to correspond with the three body points selected in the images. The Bhattacharyya distances between the distributions (or classes) are shown.
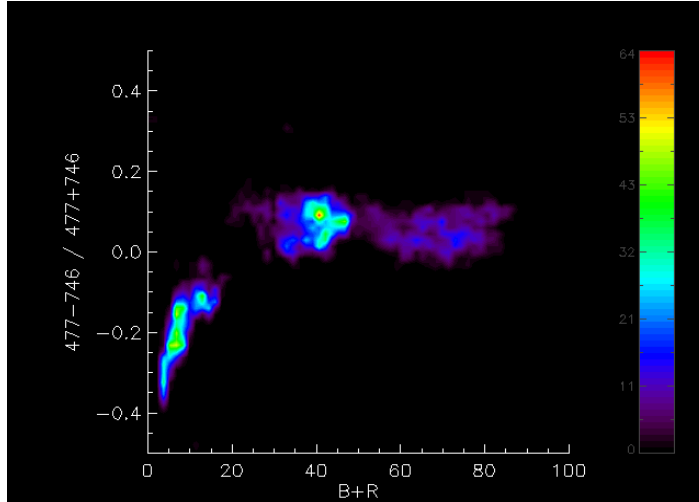
Figure 7. False-color 2D histogram of the measurements.
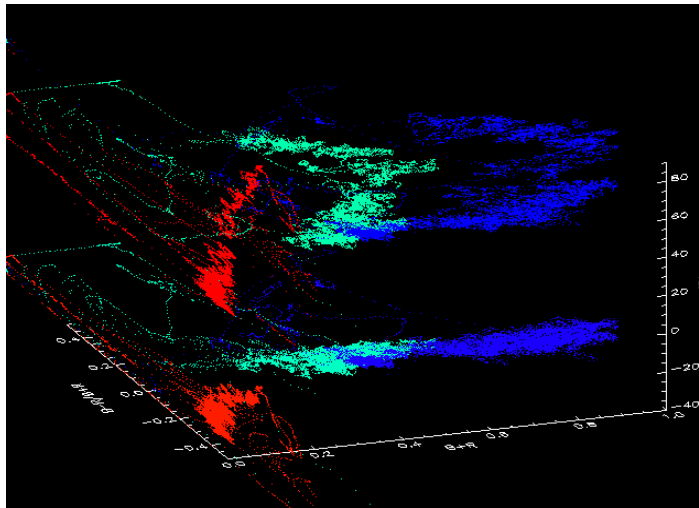

Figure 8. Measurements shown in the 3D feature space. The projection of the clouds to the horizontal (plane of constant Z) is also shown. In the 2D projection, clouds #2 and #3 are overlapped while they remain more distinguishable in 3D.
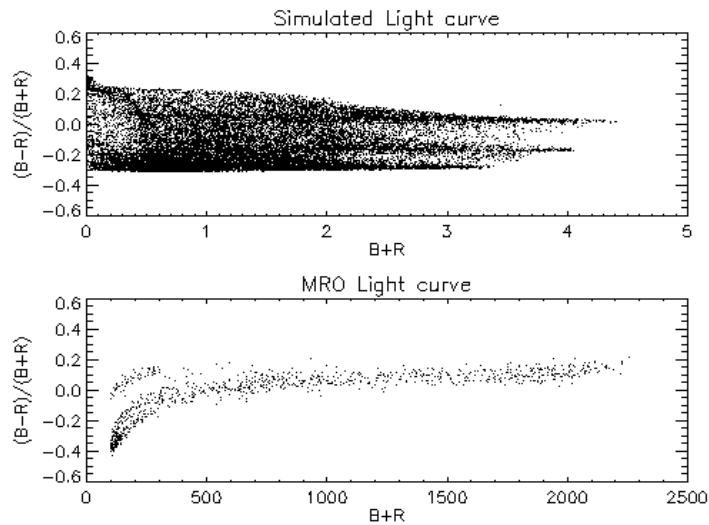
Figure 9. Helios-1B simulation is shown in upper scatter plot and measurement at the bottom.

References

[1] Lambert, J. V., LWIR Signatures of Deep Space Satellites, Specialized Data Report, MOTIF FY95-05, September 26, 1995.

[2] Payne, T. E., et al., "Modeling of Spectral Signatures from GEO Satellites (U)", Presented at the Space Surveillance Workshop, April 1996.

[3] David L. Talent, et al., "The Space Battle Lab Space Object Identification in living color", Technical Report, Feb. 2000; T.E. Payne and S. Gregory, "Filter Recommendations for Satellite Discrimination", AFRL Technical report, June 2005.

[4] P. C. Mahalanobis, "Application of statistical methods in physical anthropometry", Sankhya, vol 4, pp. 594-598, 1940.

[5] A. Bhattacharyya, "On a measure of divergence between two statistical populations defined by probability distributions", Bull. Calcutta Math. Soc., vol. 35, pp. 99–109, 1943.

[6] Morton J. Canty,"Image Analysis, Classification and Change Detection in Remote Sensing: With Algorithms for ENVI/IDL", CRC Book, August 30, 2006.